

Different ocular dominance map formation influenced by orientation preference columns

Myoung Won Cho* and Seunghwan Kim†

*Asia Pacific Center for Theoretical Physics and Nonlinear & Complex Systems Laboratory - NRL,
Department of Physics, Pohang University of Science and Technology, Pohang, Gyeongbuk, 790-784, Korea*

In animal experiments, the observed orientation preference (OP) and ocular dominance (OD) columns show various pattern types. Here, we show that the different visual map formations per species are proper crossover behavior in anisotropic systems composed of orientational and scalar components such as easy-plane Heisenberg models. We estimate the transition boundary between different pattern types and find that experimental data are consistent with our predictions.

PACS numbers: 42.66.-p, 75.10.Hk, 89.75.Fb

The highly ordered structure in the mammalian visual cortex has attracted much attention from theoretical neurobiologists and thoroughly studied in expectation of the substantiation of the neural dynamic and the computational models. Though the most models of visual map formations are based on a common postulates, such as Hebbian synapses, connections or competitions between neighbor neurons and synaptic normalization, there are quite a number of successful models with unique mechanisms [1, 2]. Recently, we showed that the visual map formations have analogy with vortex dynamics in magnetism and explained their statistical properties using the spin-like Hamiltonian models [3, 4].

As an amount of experimental data of visual maps is accumulated, people have taken an interest in the various patterns per animals with expectation of testing the different models experimentally. The observed visual patterns can be classified as at least three different types. In macaque monkeys, OD columns form parallel bands of regular spacing with relatively few branching points and mainly oriented perpendicular to area boundaries [5]. The degree of OD segregation is strong and the average typical spacing of OD, Λ_{OD} , is larger than that of OP columns, Λ_{OP} ($\Lambda_{OD} > \Lambda_{OP}$) [6]. In cats or ferrets, OD columns form an array of beaded bands exhibiting only a small tendency of elongation perpendicular to area boundaries [7, 8, 9]. The degree of OD segregation is intermediate with $\Lambda_{OD} < \Lambda_{OP}$ [10]. In the case of tree shrews, OD segregation is very weak or absent, whereas more stripe-like patterns are observed in extensive OP column regions with low densities of orientation centers [11]. Some experimental works show that the maps of orientation and ocular dominance have a number of structural relationships. The singular points, pinwheels, in OP columns tend to align with the centers of OD bands and iso-orientation contours intersect borders of OD bands at right or steep angles [6]. Such correlations between OP and OD columns occur due to the normalization of synapse strength [12]. The average response of orientation selectivity vanishes at singularities, so that strong ocular dominance can occur near pin-

wheel centers. We explained the orthogonality between contours through isotropic Heisenberg model [3]. The different visual pattern types are also originated from the synaptic normalization and the anisotropic interaction strength between two columns. The parameter λ , a measure of anisotropy between columns, turns out to be crucial in determining the pinwheel stability[3] but also OD pattern types and OP pattern regularity. We estimate the anisotropy per species from the measured typical spacing in OP and OD columns. We calculate the threshold of anisotropy between different OD patterns and compare with experimental data.

One of reasons how so many different models success in the formation of visual maps is that the typical characters of self-organizing maps are determined by the topology of lattice and feature space rather than the detailed cortical modification rules. We can guess the statistical properties of emergent cortical maps only using some mathematical constraints, such as symmetry and continuity. According to our fibre bundle map (FBM) representation method, the phases of feature components are depicted by the continuous group corresponding with the manifold in the feature space [3, 13]. Because orientation columns have $O(2)$ (or $U(1)$) symmetry, the energy functions for orientation map formations should be invariant under gauge transformations and take a general form

$$E_{OP} = \int d\mathbf{r} \left\{ \frac{v}{2} |(\nabla - i\mathbf{A})\psi_{OP}|^2 - \frac{m^2}{2} |\psi_{OP}|^2 + \dots \right\} \quad (1)$$

for the orientational feature components $\psi_{OP}(\mathbf{r}) = (q(\mathbf{r}) \cos 2\phi(\mathbf{r}), q(\mathbf{r}) \sin 2\phi(\mathbf{r}))$ (or $q(\mathbf{r})e^{2i\phi(\mathbf{r})}$) with the preferred angle $\phi(\mathbf{r})$ and the degree of preference $q(\mathbf{r})$ at cortical location \mathbf{r} . This can be obtained also from actual map formation models in a continuum approximation and explains the most typical properties of OP patterns in experiments and simulations [3].

Biologically the cortical modules are composed of several layers and the different feature components are founded on the selective response properties of corresponding layers. Each layers can have different synaptic strength and the energy of combined OP and OD map

formation takes an anisotropic form

$$E = \int d\mathbf{r} \left\{ \frac{v_{OP}}{2} |(\nabla - i\mathbf{A}_{OP})\psi_{OP}|^2 - \frac{m_{OP}^2}{2} |\psi_{OP}|^2 \right. \\ \left. + \frac{v_{OD}}{2} |(\nabla - i\mathbf{A}_{OD})\psi_{OD}|^2 - \frac{m_{OD}^2}{2} |\psi_{OD}|^2 \right\} \quad (2)$$

for the scalar component representation of ocular dominance ψ_{OD} . The imposed restriction of normalization for a total feature vector $\psi(\mathbf{r}) = (\psi_{OP}(\mathbf{r}), \psi_{OD}(\mathbf{r}))$ is that

$$|\psi(\mathbf{r})|^2 = |\psi_{OP}(\mathbf{r})|^2 + |\psi_{OD}(\mathbf{r})|^2 = \text{const} \quad (3)$$

for all \mathbf{r} . From the normalization and the equilibrium ($\nabla^2\psi_\mu \sim 0$ for $\mu = OP$ and OD) conditions, we can obtain again the orthogonality between OP and OD contour lines that

$$\nabla\psi_{OP} \cdot \nabla\psi_{OD} \sim 0. \quad (4)$$

Now, we define a parameter λ , describes the anisotropy between two columns, that

$$\lambda = m_{OD}^2/m_{OP}^2. \quad (5)$$

Then Eq.(2) has two different solutions depending on λ . If $\lambda < 1$ (or $\lambda > 1$), it has the ground state at the energy density $-m_{OP}^2/2$ (or $-m_{OD}^2/2$) with weak OD segregations $\langle\psi_{OD}^2\rangle = 0$ (or strong OD segregations $\langle\psi_{OD}^2\rangle = |\psi|^2$). The studies in magnetism show that there exist another threshold λ_c when features are composed of orientation and scalar components. The statistical properties of visual maps are closely related with those of the classical two-dimensional anisotropic Heisenberg model (CTDAHM), described by the Hamiltonian

$$H = -J \sum_{\langle ij \rangle} (S_i^x S_j^x + S_i^y S_j^y + \lambda S_i^z S_j^z), \quad (6)$$

where $J > 0$. The possibility of two vortex types, named in-plane and out-of-plane, in the CTDAHM was first discussed by Takeno and Homma [14]. Different values of the critical anisotropy λ_c , above which out-of-plane vortices are stabilized, were found to exist and depend on the lattice type ($\lambda_c \approx 0.72, 0.82, 0.62$ for square, honeycomb, and triangular lattices, respectively) by Gouv  a *et al.* [15].

For actual map formation method, we use the anisotropic Heisenberg model with distance-dependent interactions that

$$H = - \sum_{i,j} \{ D_{OP}(r_{ij}) (S_i^x S_j^x + S_i^y S_j^y) + D_{OD}(r_{ij}) S_i^z S_j^z \} \quad (7)$$

for the preferred angle $\phi_i = (1/2) \tan^{-1}(S_i^y/S_i^x)$, the ocular dominance S_i^z with normalization to a unit modulus ($|\mathbf{S}_i|^2 = 1$). The spin-like Hamiltonian model is an effective representation of neural interactions rather than the

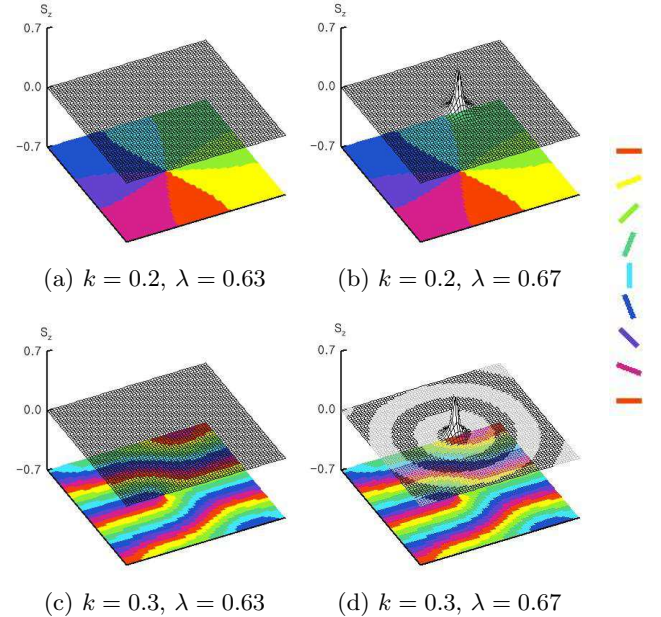


FIG. 1: Development of the scalar peak near the singularity. The preferred angle $\phi(\mathbf{r})$ is presented by 8 colors and the ocular dominance S_z is denoted with black and white wired frames, where the black denotes the region with $S_z(\mathbf{r}) \geq 0$ and the white otherwise. Simulation conditions are $\sigma_{OD}^2 = \sigma_{OP}^2 = 6$, $k_{OD} = k_{OP}$ (so $\lambda = \varepsilon_{OD}/\varepsilon_{OP}$), 60×60 lattice sizes and non-periodic boundary.

maintenance of certain neural control mechanism, such as lateral activity controls. Other development models, such as the elastic net model or Kohonen's SOFM algorithm, can be rewritten into spin-like Hamiltonian model and have common statistical properties of vortex formations [13]. In the lateral interaction scheme, $D(\mathbf{x}, \mathbf{y})$ means the neighbor connectivity itself. Usually $D(\mathbf{x}, \mathbf{y}) = D(|\mathbf{x} - \mathbf{y}|)$ takes positive for close and negative for longer distance - so called Mexican hat type. The typical parameters in Eq.(1) or (2) and the exact anisotropy λ are determined by the actual form of $D(r)$. In general, the interaction strength between each column is proportional to the activity strength ε_μ so that $\lambda \propto \varepsilon_{OD}/\varepsilon_{OP}$, and to the number of interacting pairs so that $\lambda \propto \sigma_{OD}^2/\sigma_{OP}^2$ in two-dimension for cooperation range σ_μ . In our analysis and simulations, we take the interaction function

$$D_\mu(r) = \varepsilon_\mu \left(1 - k_\mu \frac{r^2}{\sigma_\mu^2} \right) \exp(-r^2/2\sigma_\mu^2) \quad (8)$$

for a inhibitory strength k_μ and obtain the anisotropy

$$\lambda = \frac{\varepsilon_{OD}}{\varepsilon_{OP}} \frac{\sigma_{OD}^2}{\sigma_{OP}^2} \frac{k_{OD}}{k_{OP}} \exp \left(\frac{1}{2k_{OD}} - \frac{1}{2k_{OP}} \right) \quad (9)$$

for $k > k_c (= 1/4)$. Single vortex simulations in Fig. 1 show the structure of two vortex types. When λ is over

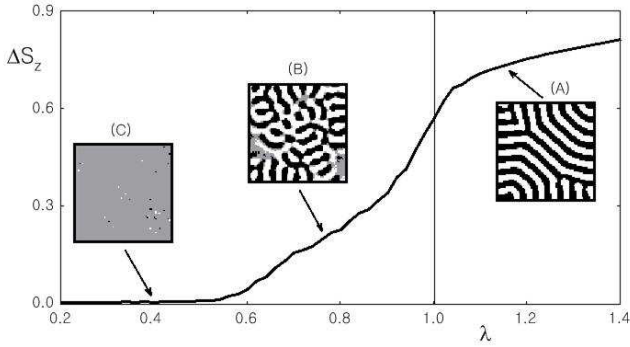


FIG. 2: (a) Different OD pattern formations and segregation strength depending on anisotropy λ . Gray color in box denotes the weak segregation region ($|S_z| \leq 0.01$). Parameters are $\sigma_{OP}^2 = \sigma_{OD}^2 = 6$, $k_{OP} = k_{OD} = 1.0$ (so $\lambda = \varepsilon_{OD}/\varepsilon_{OP}$). Maps are generated using a Metropolis algorithm at zero temperature, with a non-periodic boundary condition and an initially random state in 70×70 lattice.

than a threshold λ_c , a peak in the OD map start to develop near the singular point in the OP map (Fig. 1b & d). When there are weak inhibitory activity, they have ferromagnetic solutions and the peak in scalar component and the orientational singularity are the typical features of in-plane and out-of-plane vortices observed in the CTDAHM (Fig. 1b). Similar results can be obtained in different map formations models, but they should be modified to have anisotropy between columns if necessary.

Fig. 2 shows the emergence of three different pattern types in OD columns: (A) for $\lambda > 1$, parallel bands with strong OD segregation, (B) for $\lambda_c < \lambda < 1$, beaded bands with intermediate OD segregation, and (C) for $\lambda < \lambda_c$, the absence of OD segregation in the whole region, which correspond to observed OD patterns in macaque monkeys, cats and tree shrews, respectively. We measure the degree of OD segregation as the variation of S_z at a given time and averaged over 10 trial evolution for a given λ and find that OD segregation strength increases as λ increases. The beaded bands are not permanent structure and disappear when pinwheels annihilate in the course of progress.

For $\lambda > 1$, the Ising model region, the OD columns play a dominant role in the total map formations. Parallel bands appear in a whole range of the OD columns and make right or steep angle with area boundaries, which is the typical properties of OD maps generated without OP columns. In the OP columns, singular points and periodic patterns still exist, but are much less regular. The distribution of iso-orientation contours is not uniform with locally dense or sparse region (see Fig. 3b). The angular velocity vector $\hat{\omega}(\mathbf{r})$ defined in the feature space help to understand this. For $\lambda = 1$, the map formation progress is balanced between two stationary so-

lutions. The angular velocity vectors in feature space $\hat{\omega}$ remain slanted with $|\hat{\omega}_x| = |\hat{\omega}_y| = |\hat{\omega}_z| = 1/\sqrt{3}$ with the conservation of $\Delta S_z = \sqrt{1 - |\hat{\omega}_z|^2}/\sqrt{2} = 1/\sqrt{3} \simeq 0.577$, which can be certified in Fig. 2. For $\lambda > 1$ (or $\lambda < 1$), with the rotational plane lying more vertically (or horizontally) ΔS_z approaches 1 (or 0) as the map formation progresses. If the rotational plane becomes too slanted, the circular trajectory circles are projected to elongated ellipses and lines in the $S_x - S_y$ plane, leading to irregularities in ϕ coordinates.

In real brain, it is not certain which factor among the activity rate ε_μ , the cooperation ranges σ_μ and the inhibitory strength k_μ is a major contributor to the anisotropy between OP and OD columns. This is answered by comparing the typical spacing Λ_{OP} and Λ_{OD} measured in experiments. Besides the independent predictions in various models [3, 16, 17], the typical spacing Λ_μ would increase in proportion to the cooperation range σ_μ ($\Lambda_\mu \propto \sigma_\mu$) and decrease for stronger inhibitory strength k_μ . If OP and OD columns are different only in the activity rate ε_μ , the typical spacing are same, that is $\Lambda_{OD} = \Lambda_{OP}$ for all λ . If they differ only in k_μ , the typical spacing of OD bands is usually smaller than that of OP slabs when strong OD segregation occurs ($\Lambda_{OD} < \Lambda_{OP}$ for $\lambda > 1$). However, if they differ only in σ_μ , the typical spacing of OD bands is larger than that of OP slabs when strong OD segregation occurs ($\Lambda_{OD} > \Lambda_{OP}$ for $\lambda > 1$). Among these possibilities, the last case is mostly consistent with the animal data in cats [7, 10, 18, 19, 20], ferrets [9, 21] and macaque monkeys [6]. This leads us to conclude that the difference of cooperation ranges between columns is that the major factor which occurs typical patterns per species. Fig. 3 is simulated results using the ratio of the typical spacing Λ_μ measured in animal experiments. More beaded bands in OD columns emerge near the pinwheel centers like the visual maps in cats for $\Lambda_{OD} < \Lambda_{OP}$ (Fig. 3a), whereas parallel bands in OD columns emerge in a whole range like those in macaque

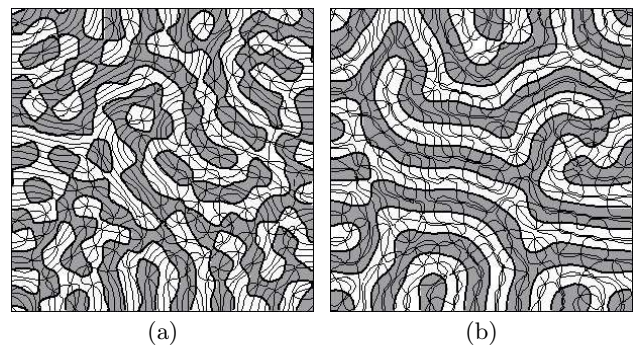


FIG. 3: Simulations of OD and OP maps for (a) $\Lambda_{OD} < \Lambda_{OP}$ ($\sigma_{OD}^2 = 6.7$, $\sigma_{OP}^2 = 10.0$) and (b) $\Lambda_{OD} > \Lambda_{OP}$ ($\sigma_{OD}^2 = 13.8$, $\sigma_{OP}^2 = 10.0$). Parameters are $\varepsilon_{OD} = \varepsilon_{OP}$ and $k_{OP} = k_{OD} = 0.7$, so $\lambda = \sigma_{OD}^2/\sigma_{OP}^2 = \Lambda_{OD}^2/\Lambda_{OP}^2$ (100×100 lattice sizes with non-periodic boundary conditions).

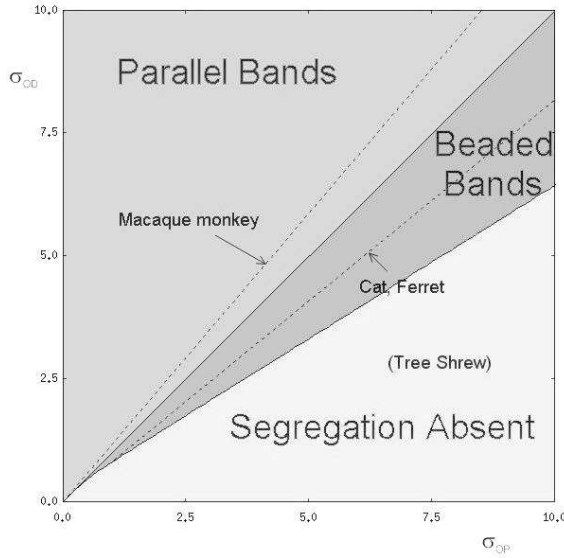


FIG. 4: The phase diagram of OD patterns according to the cooperation ranges, where the experimental data per species are also denoted.

monkeys for $\Lambda_{OD} > \Lambda_{OP}$ (Fig. 3b).

The exact calculation of the critical anisotropy λ_c , above which the out-of-plane vortices, is also an important problem in magnetism [22]. Unfortunately, any continuum theory fails in calculation of λ_c because of the singularity near the vortex core [23]. The development of out-of-plane components depends not only on the exact form of interaction function $D(r)$ but on other situations such as lattice types, vortex distributions, etc. The boundary between OD segregation absent and beaded bands regions is indistinct also in experiments and simulations because the development of OD components is weak near the boundary. We expand the analytic and simulational methods in the CTDAHM and calculate the critical anisotropy precisely for cases [24]. We find that the stability boundary of the out-of-plane vortex takes the form $\sigma_{OD} \simeq \alpha \sigma_{OP} + \beta$. Since the computed value of the β is small, the region for the beaded band pattern can be described by $\alpha < \sigma_{OD}/\sigma_{OP} < 1$ where $\alpha \sim 0.6$ when $\lambda = \sigma_{OD}^2/\sigma_{OP}^2$. This agrees well with the experimental data, where $\Lambda_{OD}/\Lambda_{OP} \sim 0.82$ for cats and ferrets. Fig. 4 shows the phase diagram of different OD pattern formations in the parameter of cooperation ranges σ_{OP} and σ_{OD} . The experimentally derived curves for macaque monkeys, cats, Ferrets lie well within regions of our predictions.

Here we show the influence of the correlation between OP and OD columns on the total map formations, and explain the experimental data successfully. Moreover, the typical characters of emergent cortical maps are just those of general fields solutions. Our studies in visual map formation mechanisms point out another possibil-

ity of physical neuron dynamic models. In spite of the complex circuitry and the nonlinear dynamics in neural systems, the neural behavior at high levels can follow more simple and general rules, which are related with the graceful theories in statistics. The cortical dynamics are not related only with the problems of cortical map formations. We expect more application of physical methodology to interpret neural phenomena and propose novel computational architecture.

This work was supported by the Ministry of Science and Technology and the Ministry of Education.

* Electronic address: mwcho@postech.edu

† Electronic address: swan@postech.edu

- [1] E. Erwin, K. Obermayer, and K. Schulten, *Neural comput.* **7**, 425 (1995).
- [2] N. V. Swindale, *Network*: **7**, 161 (1996).
- [3] M. W. Cho and S. Kim, *Phys. Rev. Lett.* **92**, 18101 (2004).
- [4] J. D. Cowan and A. E. Friedman, in *Neural Information Processing (NIPS)* (1990), vol. 2.
- [5] S. LeVay, D. H. Connolly, J. Houde, and D. C. V. Essen, *J. Neurosci.* **5**, 486 (1985).
- [6] K. Obermayer and G. G. Blasdel, *J. Neurosci.* **13**, 4114 (1993).
- [7] S. Löwel and W. Singer, *Exp. Brain Res.* **68**, 661 (1987).
- [8] P. A. Anderson, J. Olavarria, and R. C. V. Sluyters, *J. Neurosci.* **8**, 2183 (1988).
- [9] J. C. Crowley and L. C. Katz, *Nature Neurosci.* **2**, 1125 (1999).
- [10] S. Löwel, B. Freeman, and W. Singer, *J. Comp. Neurol.* **255**, 401 (1987).
- [11] W. H. Bosking, Y. Zhang, B. R. Schofield, and D. Fitzpatrick, *J. Neurosci.* **17**, 2112 (1997).
- [12] S. Grossberg and S. J. Olson, *Neural Networks* **7**, 883 (1994).
- [13] M. W. Cho and S. Kim (2004), arXiv:q-bio.NC/0405027.
- [14] S. Takeno and S. Homma, *Prog. Theor. Phys.* **64**, 1193 (1980).
- [15] M. E. Gouvêa, G. M. Wysin, A. R. Bishop, and F. G. Mertens, *Phys. Rev. B* **39**, 11840 (1989).
- [16] K. Obermayer, G. G. Blasdel, and K. Schulten, *Phys. Rev. A* **45**, 7568 (1992).
- [17] F. Hoffmeyer, F. Wolf, T. Geisel, S. Löwel, and K. Schmidt, in *Proceedings of the International Conference on Artificial Neural Networks (ICANN95)* (EC2 and Cie, Paris, 1995), vol. I, pp. 535–540.
- [18] S. Löwel, *J. Neurosci.* **14**, 7451 (1994).
- [19] K. Albus, *Exp. Brain Res.* **24**, 181 (1979).
- [20] Y.-C. Diao, J. W., S. N. V., and M. S. Cynader, *Exp. Brain Res.* **79**, 271 (1990).
- [21] S. C. Rao, L. J. Toth, and M. Sur, *J. Comp. Neurol.* **387**, 358 (1997).
- [22] J. E. R. Costa and B. V. Costa, *Phys. Rev. B* **54**, 994 (1996).
- [23] W. M. Wysin, *Phys. Rev. B* **49**, 8780 (1994).
- [24] M. W. Cho and S. Kim, *Phys. Rev. B* **70**, 24405 (2004).